Improving the Accuracy of Global DEM of Differences (DoD) in Google Earth Engine for 3-D Change Detection Analysis

Alessandra Capolupo

***Abstract*—Digital elevation models (DEMs) represent the geospatial dataset core needed to model 3-D changes. The optimal dataset must be selected according to the environmental phenomenon under investigation as the offered resolution strongly affects the information level. Nonetheless, high-resolution DEMs are not available for the whole earth and, when not at disposal, open-source, medium-resolution, global DEMs may be a relevant source of knowledge. Because of the large amount of data and the vertical accuracy inhomogeneity, their applicability in defining 3-D changes of large areas is not predictable. The aim of this article is to explore global DEMs feasibility in detecting 3-D changes at the global scale and to examine the impact of filtering propagated error on 3-D changes. To achieve these goals, a Javascript code in the Google Earth Engine environment was developed. After recognizing AW3D30 (version 3.2) and NASA SRTM DEM (version 3) as the optimal DEM combination, their DEM of Differences was computed. Such a product was affected by many of Tukey's outliers, subsequently cleaned out. Three different statistical approaches, i.e., limit of detection, uniformly distributed error, and probability map, were compared to avoid artifacts propagating further. All adopted filtering strategies improve the results reliability albeit the third one is the most effective in mountainous, urban, and rural areas. The proposed research shows that the combined use of the two above-mentioned DEMs and appropriate filtering methods allows an effective description of 3-D changes. Moreover, it outlines that such analyses are also possible by using time-saving cloud-computing platforms.**

***Index Terms*—Accuracy, DEM of Differences (DoD), digital elevation model (DEM) filtering strategies, geomatic approaches, global DEMs, Google Earth Engine (GEE).**

I. Introduction

LANDFORM mapping provides essential information to describe and model the environmental system. It allows a deeper understanding of earth's physical processes, like hydrogeological [1], geomorphological [2], and biological [3] phenomena. To this aim, analyses involving a large amount of data coming from diverse earth sciences are needed. However, in many cases, such analyses are computationally cumbersome and, thus, they drastically affect the operational time, i.e., the time required to acquire and handle the data. Over the years, several valid methods have been developed to describe the surface morphology and to also allow fast computational solving. In 1991, Moore *et al.* [4] proposed the digital elevation model (DEM) as a good compromise to provide baseline information for morphometric as well as hydrological and biological analyses and to reduce the operational time. Nowadays, DEM is recognized as the best option in performing such investigations as, beyond the above-mentioned two features, it is characterized by a peculiar property: it is a 2.5-D surface. Indeed, once the nominal terrain has been identified, a univocal elevation value is attributed to each pixel whose coordinates are defined by its horizontal position [5]. Thus, under the cartographic point of view, additionally to datum and map projection, DEM is defined by two further parameters: the planimetric grid structures (detailed by planimetric coordinates) and the elevation values (commonly expressed as ellipsoidal altitude).

DEMs ability in detecting three-dimensional (3-D) elements depends on two additional parameters, i.e., resolution and accuracy. The former pinpoints the minimal size of the object that can be investigated (the higher the resolution, the smaller the object size) [6], [7]; while the latter measures data quality. The accuracy can be distinguished in: 1) elevation accuracy, which expresses the affinity between model and actual terrain position; and 2) shape/topologic accuracy, which describes similarities between estimated model and reality. Generally, a reliable indicator of the elevation accuracy is provided by the root-mean-square error (RMSE), calculated between the DEM and the value of a set of ground control points (GCPs) [5]. Conversely, shape/topologic accuracy is commonly defined by computing DEM derivatives [5]. These two concepts are not equivalent. Indeed, small positional inaccuracy might imply erroneous shape depiction, as demonstrated in [8] and [9]. Conversely, a high autocorrelation value among elevation errors does not induce shape inaccuracy [10]. Due to the relevance of such aspects, it appears convenient to take both accuracies into account. Currently, several approaches can be adopted to evaluate DEMs quality. They can be grouped into two main categories known as "external" and "internal" validation methods, respectively. The former involves approaches that use some statistical metrics to evaluate the incoherencies between DEMs and reference datasets [11]. The latter includes methods that provide both a qualitatively and

Manuscript received October 6, 2021; revised November 4, 2021; accepted November 19, 2021. Date of publication November 23, 2021; date of current version December 13, 2021. This work was supported by the Project "Programma Operativo Nazionale Ricerca e Innovazione 2014–2020 - Fondo Sociale Europeo, Azione I.2 'Attrazione e Mobilità Internazionale dei Ricercatori' – Avviso D.D. n 407 del 27/02/2018" CUP: D94I18000220007 – cod. AIM1895471 – 2.

The author is with the Department of Civil, Environmental, Land, Construction and Chemistry, Politecnico di Bari, 70125 Bari, Italy (e-mail: alessandra.capolupo@poliba.it).

Digital Object Identifier 10.1109/JSTARS.2021.3130063

This work is licensed under a Creative Commons Attribution-NonCommercial-NoDerivatives 4.0 License. For more information, see https://creativecommons.org/licenses/by-nc-nd/4.0/

quantitatively assessment of the DEM realism by verifying the compliance of some universal rules [12]. Although the first approach is generally recognized as the best method to validate a DEM, some technical limitations are detectable [5]. These are mainly due to the restrictions in selecting the optimal reference data and to the difficulties in evaluating shape realism. Thus, the optimal strategy to identify DEM inconsistencies should be selected taking available data and coverage carefully into account. In fact, the quality assessment becomes more challenging for global DEMs even if it is supposed to be a homogeneous product. However, this represents an illusory idea as any existing methodology can globally describe surface morphology with the same accuracy level in all regions because of the variability of climate, relief, and landcover [16]. Nevertheless, those DEMs are interesting as the overall world mapping would permit a consistent global analysis.

Global DEMs production has been encouraged from technological advances, and specifically from the use of stereoscopic satellite images (since 1986) and both photogrammetric and SAR interferometric techniques [13]–[16]. Therefore, dedicated missions, such as Shuttle Radar Topography Mission (SRTM) and Advanced Spaceborne Thermal Emission and Reflection (ASTER) satellite, were released to create high-resolution products covering the world. Their accuracy was basically assessed using an external reference dataset, such as dense GCPs [17] or more accurate DEMs [18]. SRTM product, released in 2003, showed a vertical accuracy ranging between 2.18 and 21.70 m. Conversely ASTER, issued in 2006, reported a value ranging from 4.56 to 7.10 m [19], [20]. Newest freely products have been released during the last few years: 1) The Multi-Error-Removed Improved-Terrain DEM, released in 2017, showed an accuracy value comprised between 3.01 and 13.58 m. 2) The AW3D30 Global Digital Surface Model (AW3D30) Version 1, released at the beginning of 2015, has an accuracy ranging between 4.98 and 11.42 m. Data collection period lasted about five years, from 2006 up to 2011. 3) Lastly, the NASADEM, available since the beginning of 2020, reported an accuracy comprised between 6.39 and 12.08 m [21]. To improve final uncertainty, new freely available DEMs and novel versions of pre-existing models, produced by cleaning out inherent errors and artifacts, are being continuously released. For instance, the latest version of AW3D30 (version 3.2) was released in January 2021 with the aim to provide a strong quality improvement. Nevertheless, currently, its uncertainty has not been assessed yet. All these works evaluated DEMs accuracy locally, and, consequently, such statistics are not representative of the entire product and, particularly, of remote and difficult-to-reach areas. Additionally, current global DEMs are not error-free, even though the editing efforts made by space agencies and research centers in cleaning out spurious artifacts. Most of the errors are mainly introduced by the applied postprocessing procedures or the actual DEM generation technique [22].

DEM quality assessment is even more crucial in changes detection analyses (CDA) because of the error magnification, as shown in [23]. 3-D changes can be quantified through a cell-wise subtraction of DEMs corresponding to different historical periods. This procedure, known as DEM of Differences (DoD), provides relevant information about the increment or reduction in elevation of a given area [23]. DoD negative values are in general associated with geogenic activities, while positive ones are mainly linked to anthropogenic phenomena [24]. Nevertheless, distinguishing real changes from inherent artifacts is challenging. To this aim, different approaches have been developed to model and filter potential errors. In 2003, a simplified approach based on the computation of a minimum level of detection (LoD) threshold was proposed [25]. Following this approach, all DoD values higher than LoD or lower than –LoD are classified as changes, while values comprised between –LoD and LoD are assumed to be noise. However, this approach does not account for the probabilistic distribution of the error, and consequently, provides overly conservative results [23]. Subsequent improvements were proposed in [23] and [27]. A T function was used to model the error in the first study [23], while specific weight factors were assigned to the detected changes according to their relevance in [27]. The main outcome of [27] was a probability map (PM).

Results have been inspected on small test areas but, they have never been applied globally, mainly because of 1) the high computational power required in performing global scale analyses and, consequently, the inability of traditional geospatial desktop software in handling geospatial big data; 2) poor reliability of the global DEMs. The development of the Google Earth Engine (GEE) cloud platform [28], [29] released in 2017 by Google has totally altered such a scenario as it was designed to support global and local scale investigations by processing big earth observations [30]. Such a platform appears convenient thanks to its ability to parallelly process hundreds of vast information and to its integrated data archive, daily updated with nearly 6000 images collected from several sources [31]. For this reason, in the last few years, its use has rapidly grown and currently can perform both local [32]–[35] and global analyses [36]–[38]. However, its potentialities in modeling 3-D changes have not been explored yet. Indeed, although global DEMs have been incorporated in its catalog, GEE suffers from the lack of specific calculation methods [39]. Existing algorithms are devoted to terrain information computation, such as slope, illumination, and curvature [39].

The present research was conceived in such a theoretical framework with the aim to assess whether open-source global DEMs, coupled with appropriate filtering strategies, can be used to detect 3-D changes that occurred between 2000 and 2011 at a global scale. In this study, 3-D changes are described as latitude–longitude position plus altimetry. To meet such purposes, a specific GEE code was developed. The most suitable global DEMs among SRTM DEM V3, NASADEM, AW3D30 version 2.2, and AW3D30 version 3.2 were compared through statistical comparison tests. Once DEMs were selected and DoD was calculated, three DoD filtering strategies, i.e., limit of detection (LoD), uniformly distributed error (UDE), and PM were applied. Their results and the corresponding impact on CDA were evaluated. Such an investigation allowed exploration of the GEE environment performance in processing geospatial big data.

The rest of this article is organized as follows. Section II deepens the methodology. Specifically, Sections II-A and II-B introduce the dataset and its quality assessment, whereas

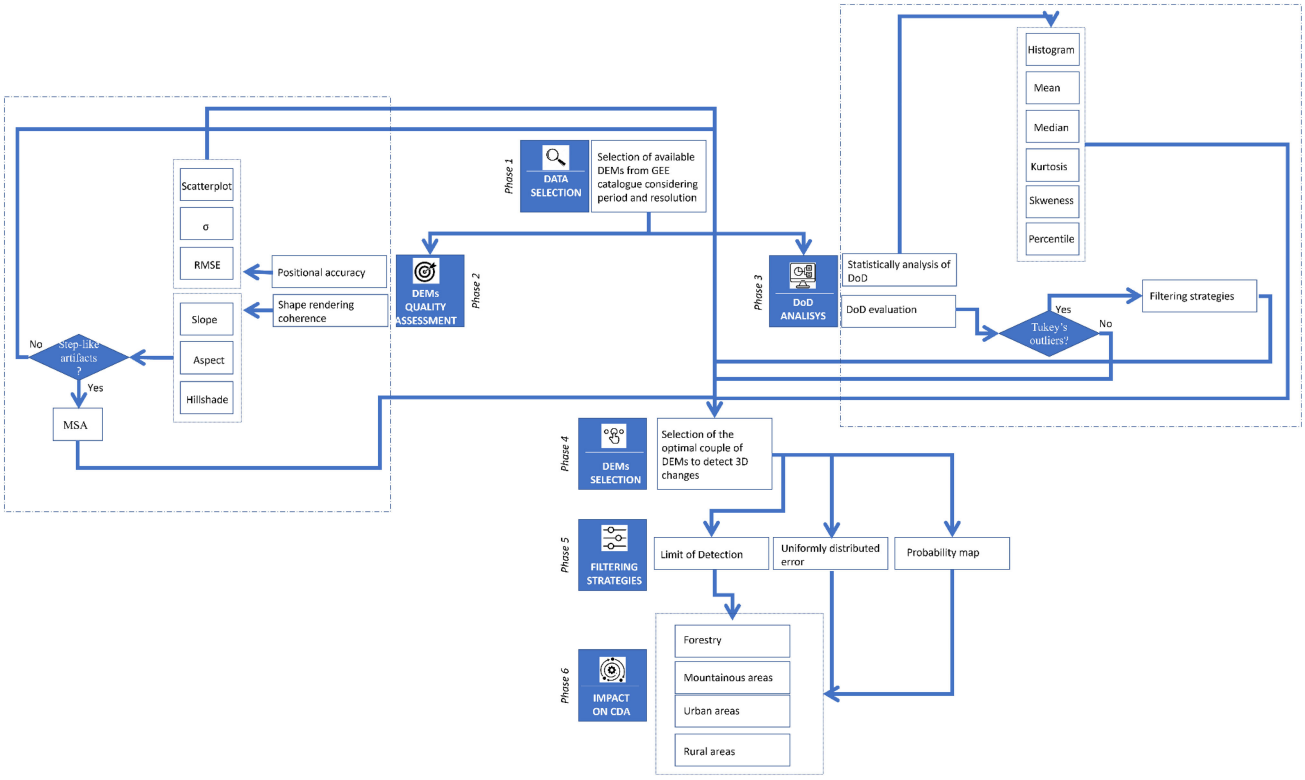

Fig. 1. Operative workflow to assess the impact of filtering strategies on 3-D changes at global scale using open-source global DEMs within the GEE framework.

Sections II-C, II-D, and II-E analyze the theory of DoD and of combined error propagation, enhancing potentialities and constraints of each proposed approach. Sections III and IV, respectively, present and discuss the results. Finally, Section V concludes this article.

II. Methodology

This section illustrates the procedure adopted to meet the research purposes, which are also illustrated in Fig. 1. Particularly, the procedure can be broken down into the following six main phases.

1) Database construction and implementation in GEE.
2) DEMs quality assessment.
3) DoD computation.
4) Global DEMs selection.
5) Error modeling and filtering.
6) Evaluation of filtering strategies impact on CDA.

Specifically, after having detected the most suitable global DEMs available in the GEE catalog (Phase 1) and assessed their quality (Phase 2), the corresponding DoDs were computed and statistically investigated (Phase 3). By combining the observations produced in Phases 2 and 3, the optimal DEM-combination that provides the best description of 3-D changes was selected (Phase 4). Due to error propagation into a DoD, three different statistical strategies were used to model and filter the combined noise (Phase 5). Once the filtering phase was completed, the impact of each strategy on CDA was detected at a global scale (Phase 6).

A. Data Sources and GEE Database Construction (Phase 1)

The following four open global DEMs with a comparable spatial resolution (1 arcsecond – 30 m) were selected as data test.

1) NASA SRTM DEM V3.
2) NASADEM.
3) AW3D30 (version 2.2).
4) AW3D30 (version 3.2).

SRTM DEM was obtained by processing the images collected between 60 l°N and 60°S for 11 days in February 2000 by two synthetic aperture radars mounted on Space Shuttle Endeavour: a C radar (5.6 cm) and an *X*-band system (2.2 cm), respectively [41], [42]. The former was adopted for producing a global map; the latter, instead, was integrated as an experimental exhibition because of its capability of acquiring pictures with slightly higher resolution and better signal-to-noise ratio than the other system although along narrow swaths 50 km wide [39]. Thus, it was used to improve the quality of the data acquired by the C radar and the final accuracy was equal to 16 and 9 m horizontally and vertically, respectively [40], [41]. Nevertheless, some studies reported a higher vertical accuracy in mountain regions (4.31 m – ±14.09 m) [43]. SRTM DEM version 3 (SRTM DEM V3), released by NASA Jet Propulsion Laboratory in 2014 and already implemented in the GEE catalog, was adopted in this research [46]. Contrary to the other previous versions in which voids were filled by using commercial datasets, a void-filling process based on open-source data was carried out for SRTM DEM V3. Its accuracy was certified to be between 2.18 and 21.70 m [19], [20].

TABLE I
SUMMARY OF THE GLOBAL DEMS FEATURES CONSIDERED IN THE PRESENT RESEARCH

Dataset	Spatial resolution [m]	Method	Collection period	Estimated vertical accuracy [m]
SRTM DEM V3	30	Interferometry synthetic aperture radar	2000	2.18 - 21.70
NASADEM	30	Interferometry synthetic aperture radar	2000	6.39- 12.08
AW3D30 VERSION 2.2	30	Photogrammetry	2006-2011	5
AW3D30 VERSION 3.2	30	Photogrammetry	2006-2011	/

NASADEM is considered as the successor of SRTM DEM, although it is not based on its latest version (i.e., version 3). In fact, it involves advanced procedures, software, and reference additional data, as ASTER, ICESat, and GLAS to fill voids of SRTM DEM Version 2. Therefore, although any previous studies systematically estimated its overall vertical accuracy, Uuemaa *et al.* [21] detected such a parameter in three study areas: Estonian (6.39 m), China (8.53 m), and New Zealand (12.08 m). In all regions, its accuracy was slightly higher than SRTM DEM V3.

AW3D30 was extracted by processing stereoscopic images collected between 2006 and 2011 by the Panchromatic Remote-Sensing Instrument for Stereo Mapping, an optical sensor mounted on the Advanced Land Observing Satellite [47]. Released in 2016 first, this dataset has been continually updated over the years by applying different calibrations and void filling procedures [47]. In this research, two AW3D30 versions were considered: 2.2 (released in April 2019) and 3.2 (January 2021), respectively. To the best of my knowledge, no previous research evaluated the accuracy of AW3D30 version 3.2, in the following named as AW3D30 (3.2); conversely, AW3D30 version 2.2, in the following called as AW3D30 (2.2), provides an accuracy equal to 5 m both in geolocation and height [48]. That result depends mainly on the automatic identification and remotion of clouds, snow, and ice during the image processing phase even though height errors are still detectable close to the pixels surrounding such areas. Additional details about these data are reported in Table I.

Such data were stored in the GEE catalog which is daily updated with nearly 6000 publicly available geospatial datasets, collected by different platforms [29], [44]. All users may access them and select the data meeting their needs through the application programming interface (API). Thus, after detecting the most suitable information, they can be directly imported into the JavaScript application and handled on the cloud. This allows exploiting the great computational potentialities of that platform. Anyway, once the data were selected and the database constructed in the JavaScript API, a programming code was developed to estimate DEMs accuracy and evaluate the 3-D changes that occurred over the period between 2000 and 2011.

B. DEM Quality Assessment (Phase 2)

The quality of the selected DEMs was assessed to detect the main incongruencies and inconsistencies existing within them. This step allows detecting the most suitable DEMs to perform the CDA over the period 2000–2011. In fact, as underlined in the previous paragraph, the overall accuracy of AW3D30 (3.2) is unknown. Therefore, to select which products to implement in the following processing steps, it is essential to define its performance. To meet such a need, the internal validation procedure, i.e., visual control, was preferred to the external validation method because of the lack of reference data. Although this inductive approach is commonly neglected, it is recognized as a powerful tool to easily validate a DEM [12].

First, position accuracy among DEMs extracted from the same source was assessed through statistical analysis. It was expected that NASADEM and AW3D30 (3.2) statistically preserve or, at least, improve the absolute position accuracy of SRTM DEM and AW3D30 (2.2), respectively. A scatterplot, providing information regarding their correlation and their spatial distribution, and the most relevant statistics (standard deviation (σ) and RMSE) were estimated from their difference. Then, their shape rendering coherence was also evaluated, extracting their derivatives (aspect, slope, and hillshade) using the ee.Terrain package [49]. The aspect quantifies the direction of the maximum slope. Thus, such a parameter is particularly useful to evaluate the noise on flat areas or on drainage networks. On the contrary, the slope represents the maximum rate of change between a cell and its eight neighboring cells. It pinpoints DEM inherent inconsistency due to elevation discrepancies among neighboring cells. Therefore, it is especially effective in assessing the presence of step-like artifacts, such as sinkholes and line error, in the mountainous areas rich in drainage networks. The hillshade is obtained by illuminating a surface with a virtual light, placed on the northern side. This results in illuminating the screen from the top to the bottom which allows detecting the real land surface. Generally, a greyscale map is used to illustrate its outcome. The variation of the grey levels depends on slope change. As a consequence, hillshade appears more effective than DEM to identify gross errors and resampling artifacts in the raster. All the above-mentioned geomorphological descriptors were evaluated in mountainous zones characterized by a large amount of drainage networks to maximize their effectiveness. The trend of each data was investigated both visually and statistically. Lastly, to remove the step-like artifacts, the maximum slope approach was applied [22]. Such artifacts, e.g., cell defects, line error, sinkholes, and steps at the shoreline are usually considered as gross errors in the DEM heights which may largely influence subsequent analyses. Such phase was recognized as essential since gross errors cannot be considered normally distributed.

C. DoD Computation and DEMs Selection (Phases 3 and 4)

In this study, the DEM differencing procedure [23], also known as DoD [50], was applied to explore the 3-D changes at a global scale. It consists of the following four main steps.

1) Computing a DoD by subtracting the later (DEM_2) and the earlier (DEM_1) collected DEMs (1).

2) Estimating error propagation into a DoD.
3) Filtering the error.
4) Detecting and analyzing changes

$$\mathrm{DoD} = \mathrm{DEM}_2 - \mathrm{DEM}_1 \tag{1}$$

The DoD construction phase was straightforward: it was programmed as a raster difference between the two input DEMs exploiting available GEE instructions. Conversely, the second step was demanding both in terms of models to be adopted and programming code to be developed. First, a statistical approach was implemented to identify and then clean out the outliers using Tukey's method [51]. Tukey's method is largely recognized as a powerful tool to remove inherent noise because of the lack of any *a priori* distribution assumptions. Lastly, the probabilistic theory proposed by Taylor in 1997 [52], detailedly described in the following section, was implemented as well as all the approaches developed from it over the years.

After filtering the noise, 3-D changes were explored. The resultant DoD can show negative, positive, or equal to zero values: the former corresponds to those areas which experienced a reduction of elevation mainly due to natural hazards; the second ones dovetail those zones characterized by an increment of elevation, essentially triggered by human activities; and, lastly, zero values are related to those areas stable over the time [52]. Those indications are effective when DEM_1 is referred to an earlier period than DEM_2.

Thus, the optimal couple of DEMs to detect 3-D changes was selected by integrating the outcomes of this phase with the one achieved in the previous step.

D. Probabilistic-Based Theory for Error Propagation Into a DoD (Phase 5)

In 1997, Taylor developed the probabilistic-based theory for error analysis in [52]. It is assumed that a variable (x), affected by only random errors, is normally distributed and, thus, it can be described using two parameters: average (μ) and standard deviation (σ). Consequently, supposing the true values of x (X) are equal to 0, (2) describes the probability of identifying any values of x

$$\mathrm{Prob}\ (x) \propto \exp\left(-\frac{x^2}{2\sigma_x^2}\right). \tag{2}$$

Introducing a second independent and normally distributed variable (y), the probability to simultaneously compute x and y is

$$\begin{aligned}\mathrm{Prob}\ (x,\ y) &\propto \exp\left(-\frac{x^2}{2\sigma_x^2}\right)\ \exp\left(-\frac{y^2}{2\sigma_y^2}\right)\\ &= \exp\left[-\frac{1}{2}\left(\frac{x^2}{\sigma_x^2}+\frac{y^2}{\sigma_y^2}\right)\right]\\ &= \exp\left[-\frac{1}{2}\left(\frac{(x-y)^2}{\sigma_x^2+\ \sigma_y^2}+\frac{\left(\sigma_x^2 y+\sigma_y^2 x\right)^2}{\sigma_x^2\sigma_y^2\left(\sigma_x^2+\ \sigma_y^2\right)}\right)\right]\end{aligned} \tag{3}$$

which can be rewritten as

$$\begin{aligned}\mathrm{Prob}\ (x-y,\ z) &\propto \exp\\ &\times\left[-\frac{1}{2}\left(\frac{(x-y)^2}{\sigma_x^2+\ \sigma_y^2}\right)\right]\left[-\frac{1}{2}\left(\frac{\left(\sigma_x^2 y+\sigma_y^2 x\right)^2}{\sigma_x^2\sigma_y^2\left(\sigma_x^2+\ \sigma_y^2\right)}\right)\right]\end{aligned} \tag{4}$$

with z the term reported in the second brackets; conversely, the first factor expresses the probability of getting any values of the variable x–y, normally distributed and with an uncertainty (δ) of

$$\delta = \sqrt{\sigma_x^2+\ \sigma_y^2}. \tag{5}$$

This theory represents the base of the three widely adopted approaches developed to detect and filter the noise into a DoD, which are detailed in the following sections. Each theory introduces specific modifications to improve the effectiveness of the results.

E. Limit of Detection

The first strategy considers the uncertainty δ in each DEM cell as a random and independent variable. As proved in [26], assuming $x = \mathrm{DEM}_2$ and $y = \mathrm{DEM}_1$, δ can be always adopted to evaluate the uncertainty propagation into a DoD at a global scale; while, for local scale analysis, it can be used only if $\sigma_x = \sigma_y$. Thus, the combined error in a DoD can be estimated as a single value by applying (5), which is called LoD. LoD is used to thresh the DoD and all smaller values than LoD and higher than –LoD are considered as noise and thus discharged. Nevertheless, this approach is affected by an intrinsic issue: the probabilistic nature of the DoD error is totally missed and, thus, relevant information could be lost. Based on these considerations, Brasington *et al.* [54] developed an alternative approach, described in the following.

F. Uniformly Distributed Error

This methodology considers a user-defined confidence interval by introducing a T-student statistic (t). It accounts for both Gaussian and not Gaussian distribution [55], [56] using the following new threshold:

$$U_{\mathrm{critical}} = t{*}\delta. \tag{6}$$

The value of t is a function of the desired confidence interval. In particular, t is set to 1.00 and 1.96 for a confidence interval of 68% and 95%, respectively. As in the previous procedure, an average value of the standard deviation is used to describe the error in each DEM. Thus, also this approach uses a uniform threshold to classify noisy information. As a consequence, the threshold is not locally fixed and, therefore, this technique may overestimate or underestimate the amount of information to filter. This results in losing relevant data or not adequately cleaning the noise. In this sense, it does not allow one to explore the potentiality of the t probabilistic distribution. As also this filtering strategy is affected by some limitations, Lane *et al.* [26] proposed a third strategy, which is reported in the following.

G. Probability Map

This approach does not discharge noise using a uniform threshold, but it is based on a PM. A weight ranging between 0

TABLE II
STATISTICS COMPARISON AMONG SELECTED DATASET USING Σ (STANDARD DEVIATION) AND RMSE

DATASET	PEARSON'S COEFFICIENT	σ	RMSE [m]
NASADEM – SRTM DEM V3	0.9997	19.33	19.00
AW3D30 2.2- AW3D30 (3.2)	0.9997	22.61	20.51
NASADEM- AW3D30 (2.2)	0.9996	26.07	25.69
NASADEM- AW3D30 (3.2)	0.9996	25.18	24.80
SRTM DEM V3 - AW3D30 (2.2)	0.9992	37.58	37.02
SRTM DEM V3 - AW3D30 (3.2)	0.9992	24.61	23.40

and 1 is assigned to each DoD pixel according to its statistical significance. For instance, 1.0 is attributed to all elevation values having a confidence interval of 95%, 0.5 to pixels showing a confidence interval between 68% and 95%, and 0 to points with a confidence interval smaller than 68%. The resulting PM is used to weight the DoD layer, cleaning out the combined error.

H. Filtering Strategies Impact on CDA (Phase 6)

In the proposed research, specific computational algorithms were used to implement these three filtering strategies within the GEE framework to assess their impact on CDA. Specifically, their performances were assessed by comparing the results with the ones obtained by inspecting Google Earth Pro images. Thanks to a time-lapse tool, this application provides high-resolution images corresponding to different periods. After selecting images acquired over the period 2000–2011, the interpretation phase was carried out. To fully explore the potentialities of the three adopted filtering methods, different scenarios were investigated including urban, mountainous, forestry, and rural areas as well as zones characterized by many outliers.

III. RESULTS

A. Global DEMs Accuracy Evaluation and DoD Selection

As described in Section II-B, global DEMs were statistically compared by computing Pearson's coefficient, RMSE, and σ in order to assess their ability in capturing 3-D changes (see Table II). As the main outcome, a strong correlation between all examined data can be noted by looking at the Pearson coefficient (i.e., 0.99). Its value underlines the presence of elevation coherence among points located in the same position. Furthermore, the two remaining statistical variables (i.e., RMSE and σ) enhance a not-uniform vertical accuracy as the committed errors are affected by a heterogeneous spatial distribution. Looking in detail at RMSE and σ, the couple consisting of AW3D30 (2.2) and SRTM DEM V3 provided the worst results, mainly because of the two reasons: 1) 3-D changes occurred in the investigated period (2000–2011) and, 2) inherent inconsistencies and artifacts. Although a slight improvement could be achieved with the use of the AW3D30 DEM latest version (3.2), a large dispersion and a high committed error are also shown by the couple SRTM DEM V3 and AW3D30 (3.2). Similarly, the groups NASADEM – AW3D30 show high RMSE and σ values albeit a smaller reduction of these parameters can be seen using the latest AW3D30 version. Importantly, the combination NASADEM – SRTM DEM V3 as well as AW3D30 (3.2) – AW3D30 (2.2) report the best performance. This can be easily explained since NASADEM and AW3D30 (3.2) are just improved versions of the other two.

The main outcome of this Phase 2 was that SRTM DEM V3 – AW3D30 (3.2) appeared as the best combination to investigate 3-D changes.

A further in-depth statistical analysis involving these datasets and their combination was performed. The corresponding results are illustrated through boxplots in Figs. 2 and 3, which allow to synthesize their tendencies. Specifically, Fig. 2 reports the global DEMs boxplots, whereas Fig. 3 reports the DoD ones.

Looking at Fig. 2, all DEMs statistics are represented through a compressed box, many positive outliers, and different interquartile ranges, confirming the results reported in Table II. As can be noted, all DEMs have a similar trend albeit a big dispersion among values, identified by a large number of positive outliers and wide interquartile ranges. Relevant additional information can be also inferred: dispersion is mainly concentrated over mountainous and forestry zones as outliers are located at the highest elevation values.

Looking at specific DEMs pairs, additional information can be deduced. Both versions of AW3D30 show slightly higher elevation values than the other analyzed products. Such error was partially corrected in the 3.2 version. Similarly, because of the correction procedures, NASADEM shows higher elevation values than SRTM DEM V3. These considerations are also supported by the DoD boxplots of Fig. 3. For instance, looking at AW3D30 (3.2) and AW3D30 (2.2) boxplots [see Fig. 3(c)], most of the values are close to 0 and only a few positive outliers can be seen. Consequently, the two DEMs are pretty overlapping even though the latest version shows an elevation reduction, as highlighted by positive outliers. AW3D30 products report higher values than the SRTM DEM V3, while NASADEM shows lower values than AW3D30 (2.2) and higher values than AW3D30 (3.2).

Such considerations are also confirmed by the DoD histograms reported in Fig. 4. As expected, the highest peak is roughly centered around 0 albeit a large dispersion of values is caught. Their data trends deviate from a normal distribution because of a statistically significant skewness and kurtosis; meaning that they all show a disequilibrium between negative and positive values, which are associated with an elevation reduction and increment, respectively. This disequilibrium is not homogeneous. For instance, looking at the couple AW3D30 (3.2) and AW3D30 (2.2), the DoD is essentially characterized by negative values while the pair NASADEM – SRTM DEM V3 is mainly composed of positive factors. Conversely, a more stable situation is shown by the couple AW3D30 (3.2) - SRTM DEM V3 as well as AW3D30 (2.2) - SRTM DEM V3. Table III summarizes the main parameters describing DoD distribution.

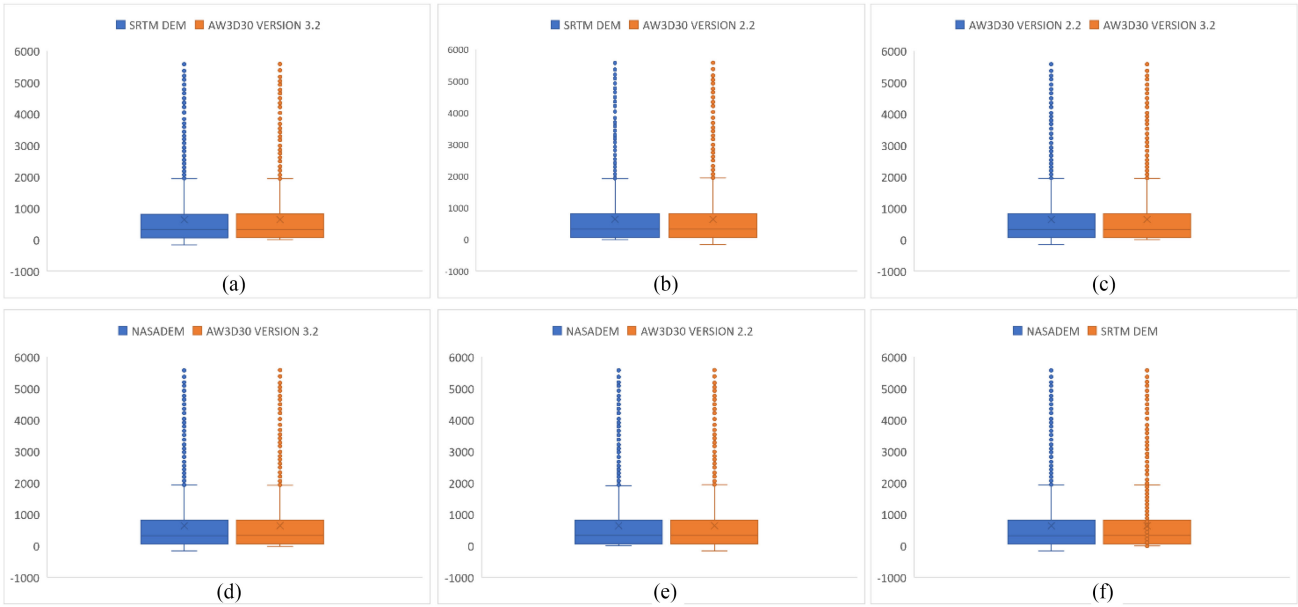

Fig. 2. Boxplot of global DEM. (a) SRTM DEM V3 (blue) and AW3D30 (3.2) (orange). (b) SRTM DEM V3 (blue) and AW3D30 (2.2) (orange). (c) AW3D30 (2.2) (blue) and AW3D30 (3.2) (orange). (d) NASADEM (blue) and AW3D30 (3.2) (orange). (e) NASA DEM (blue) and AW3D30 (2.2) (orange). (f) NASADEM (blue) and SRTM DEM V3 (orange).

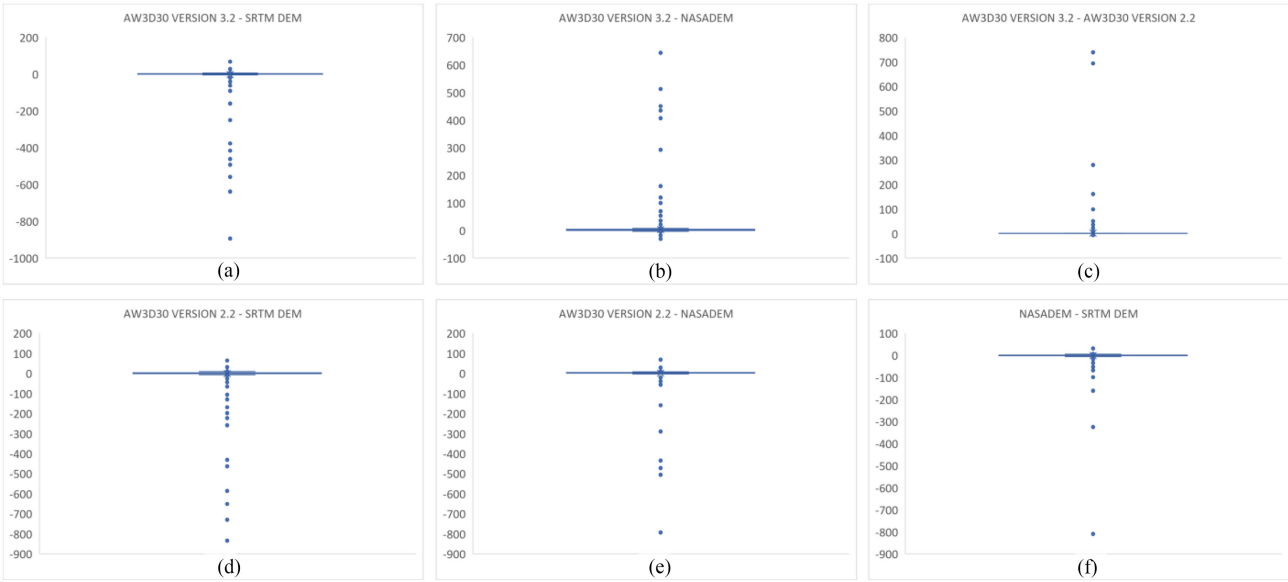

Fig. 3. DoD boxplot. (a) AWD30 (3.2) and NASA SRTM DEM V3. (b) AWD30 (3.2) and NASADEM. (c) AWD30 (3.2) and AWD30 (2.2). (d) AWD30 (2.2) and NASA SRTM DEM V3. (e) AWD30 (2.2) and NASADEM. (f) NASADEM and NASA SRTM DEM V3.

This additional statistical analysis confirms what was deduced in Phase 2: AW3D30 (3.2) and SRTM DEM V3 represent the optimal couple to investigate 3-D changes, and, therefore, they will be used in the further CDA.

Data realism was also evaluated by computing DEMs derivatives (hillshade, aspect, and slope). Topological and geometrical errors can be easily detected in mountainous areas characterized by a large amount of drainage networks. Thus, a zone with these features was selected to illustrate this aspect (see Fig. 5). Graduate color and grey maps were adopted to depict elevation and DEMs derivatives, i.e., slope, hillshade, and aspect, respectively. Most of the information regarding inherent artifacts are provided by the aspect layer [see Fig. 5(d)] that clearly shows the presence of noise in the drainage network of AW3D30 (2.2). Such problems have been totally cleaned out with its latest version, i.e., AW3D30 (3.2), which shows significant overall improvements. Indeed, lake errors are not detectable in SRTM DEM V3, NASADEM, and AW3D30 (3.2) since the water bodies were masked during the editing phase. These improvements justify the large statistical difference between them highlighted

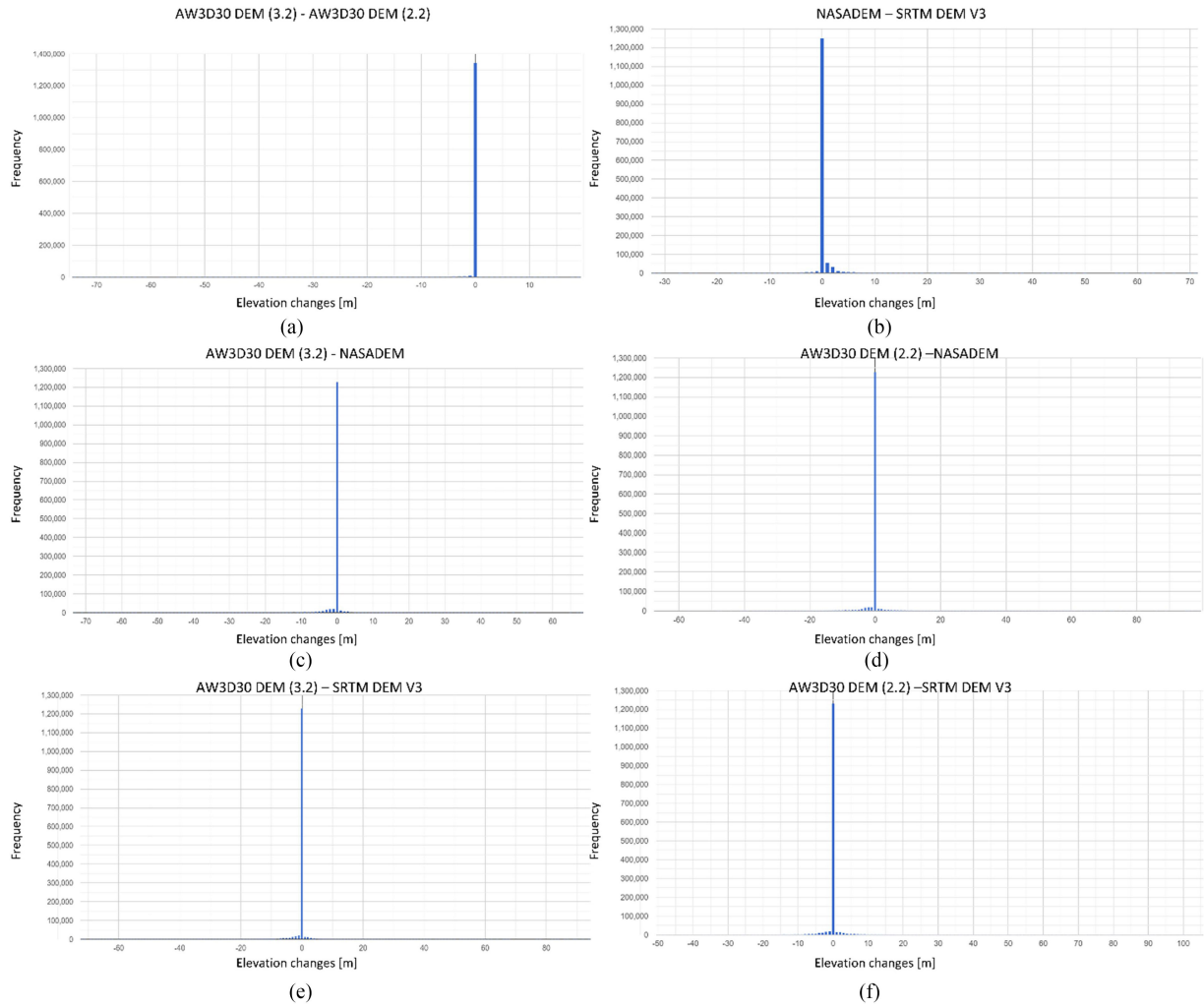

Fig. 4. Histograms of DoDs computed for each investigated couple.

TABLE III
DoDs Statistics

DoD	Mean	Median	Skweness	Kurtosis	Per [25]	Per [90]
NASADEM – SRTM DEM V3	-0.64	2.36	-0.0037	93.88	-5.70	22.50
AW3D30 (3.2) – AW3D30 (2.2)	-0.30	2.77	0.42	29.56	-5.67	22.51
AW3D30 (2.2) – NASADEM	1.29	2.85	0.16	93.80	-5.14	22.09
AW3D30 (3.2) – NASADEM	1.10	3.13	0.45	29.73	-5.80	22.38
AW3D30 (2.2) – SRTM DEM V3	0.42	1.34	3.00	29.82	-2.13	1.34
AW3D30 (3.2) – SRTM DEM V3	0.12	2.80	0.45	30.03	-5.71	22.51

in Table II. Coherently, the hillshade extracted using AW3D30 (3.2) is smoother than the one obtained with AW3D30 (2.2), as shown in Fig. 5(c), whereas any relevant information can be deduced from slope [Fig. 5(b)] and elevation [Fig. 5(a)] layers. Such an improvement cannot be seen comparing SRTM DEM V3 and NASADEM derivatives [see Fig. 5(d)], even though the latter is commonly considered as the latest SRTM DEM version. In detail, at this site, the correction procedures implemented in NASADEM affect only the vertical accuracy without improving data realism.

Based on the previous analyses, the DoD obtained subtracting SRTM DEM V3 from AW3D30 (3.2) appears as the best option to perform CDA at a global scale. Fig. 6 illustrates Tukey's outliers with red points, which as expected are mainly located over mountainous and forestry areas. For this reason, a preprocessing step aimed at identifying and cleaning out all detected outliers is needed.

B. Error Filtering Strategies Effects

The three filtering strategies adopted are LoD, UDE, and PM. 3-D changes of the earth and filter's ability can be difficult appraised considering simultaneously overall the world due to its size. To illustrate how appropriate filtering strategies can be used to detect 3-D changes in diverse areas, six explanatory pilot

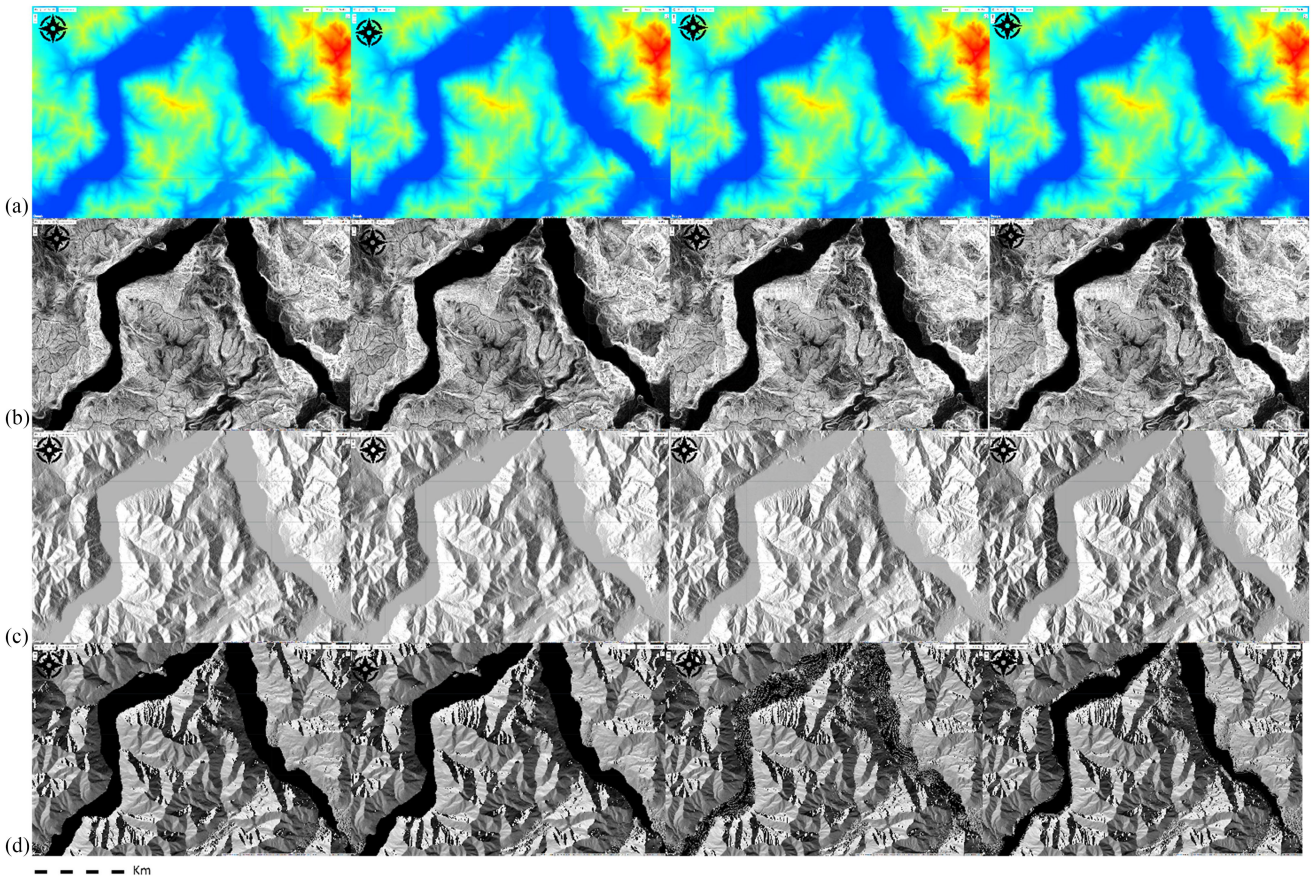

Fig. 5. DEM realism assessment by comparing (a) elevation, (b) slope, (c) hillshade, and (d) aspect with, from left to right, SRTM DEM V3, NASADEM, AW3D30 (2.2), and AW3D30 (3.2). Pilot site: Lago di Como (Italy) (5084511.36 N, 518119.12 E).

Fig. 6. Tukey's outliers highlighted with red points on Google Earth map.

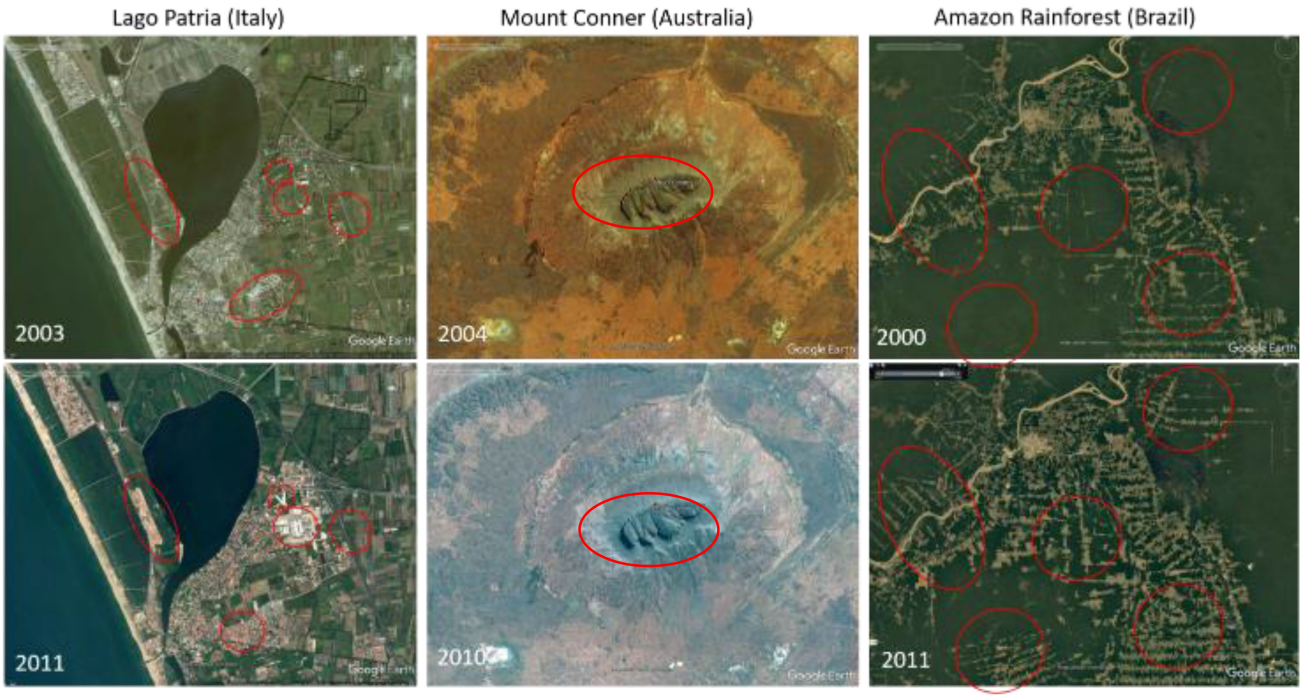

Fig. 7. Satellite images acquired from Google Earth Pro in two distinct periods and corresponding to the three nonurban pilot sites: Lago Patria – Italy (4531864.01 N, 418589.67 E), Mount Conner – Australia (7176935.21 S, 791561.79 E), and Amazon Rainforest - Brazil (8894235.45 S, 421113.78 E). 3-D changes occurred in the considered period are outlined with red circles.

sites were selected and grouped into two categories. The first one (see Figs. 7 and 8) looks at the changes in nonurban areas and three zones are selected: Lago Patria (Italy), Mount Conner (Australia), and Amazon Rainforest (Brazil). Conversely, the second group (see Figs. 9 and 10) aims at showing the performance of the proposed strategies on urban areas (Paris, France and New York, USA) and on a mountainous zone with many outliers (Northern England). Figs. 7 and 9 were introduced to geographically localize the selected pilot sites.

Referring to nonurban areas, Fig. 7 shows the three selected areas as they appeared in two distinct periods, whereas in Fig. 8, the results using the three filtering strategies are reported. Specifically, the first row of Fig. 8 illustrates the DoD, the second row reports the LoD, the third and fourth rows show the UDE using two different confidence intervals (68% and 95%, respectively), while the last row reports the PMC analysis. Looking at Fig. 7, the main changes are denoted with red circles. It is worth noting that the mountainous area (Mount Conner) is not affected by relevant changes while both the rural (Lago Patria) and the forestry (Amazon Rainforest) zones show significant transformations.

Large areas of changes are observed using LoD and UDE approaches. Importantly, the LoD does not allow to change the threshold and thus to adapt the analysis to specific areas conditions. Indeed, it overestimates the changes in forestry and mountainous areas while it correctly classifies conversions in rural zones. Generally, UDE is more effective even though the confidence interval of 95% is not sensitive at the transformation on cultivated surfaces while the confidence interval of 68% is not satisfying in mountainous and forestry sites. Thus, the two intervals appear complementary. PMC integrates the information provided by the two confidence intervals and, thus, it allows to categorize changes in probability.

Specific attention should be deserved to urban areas and those zones characterized by many outliers, mainly located along the coastline. Similarly, to mountainous and forestry areas, the UDE approach based on the 95% confidence interval is the most performant (Fig. 10(d)—Paris, France and New York, USA). In fact, it allows detecting the most relevant variation, circled in red in Fig. 9, as well as street trees changes. Conversely, the LoD method and the UDE technique with a confidence interval of 68% overestimate the changes, and, thus, their results are untreatable in such areas [see Fig. 10(c) and (d)]. Lastly, the effectiveness of both methods is not sufficient in areas showing many outliers (see Fig. 9—Northern England). It is worth noting that the PM plays a crucial role to interpret changes thanks to the use of appropriate weight factors [see Fig. 10(e)].

IV. Discussion

Detecting changes at a global scale is still challenging despite the great amount of open data released in the last decades. This is essentially due to two main aspects: the difficulties in processing geospatial big data and the poor reliability of open-source global DEMs. To overcome these limitations, this research has been focused on the combination of GEE [27], a recently released cloud computing platform, and the introduction of statistical approaches to filtering the propagated error. Because of the power due to parallel computing, GEE is favoring new advancements in remote sensing fields allowing real-time handling of geospatial big data even in large areas [29], [30].

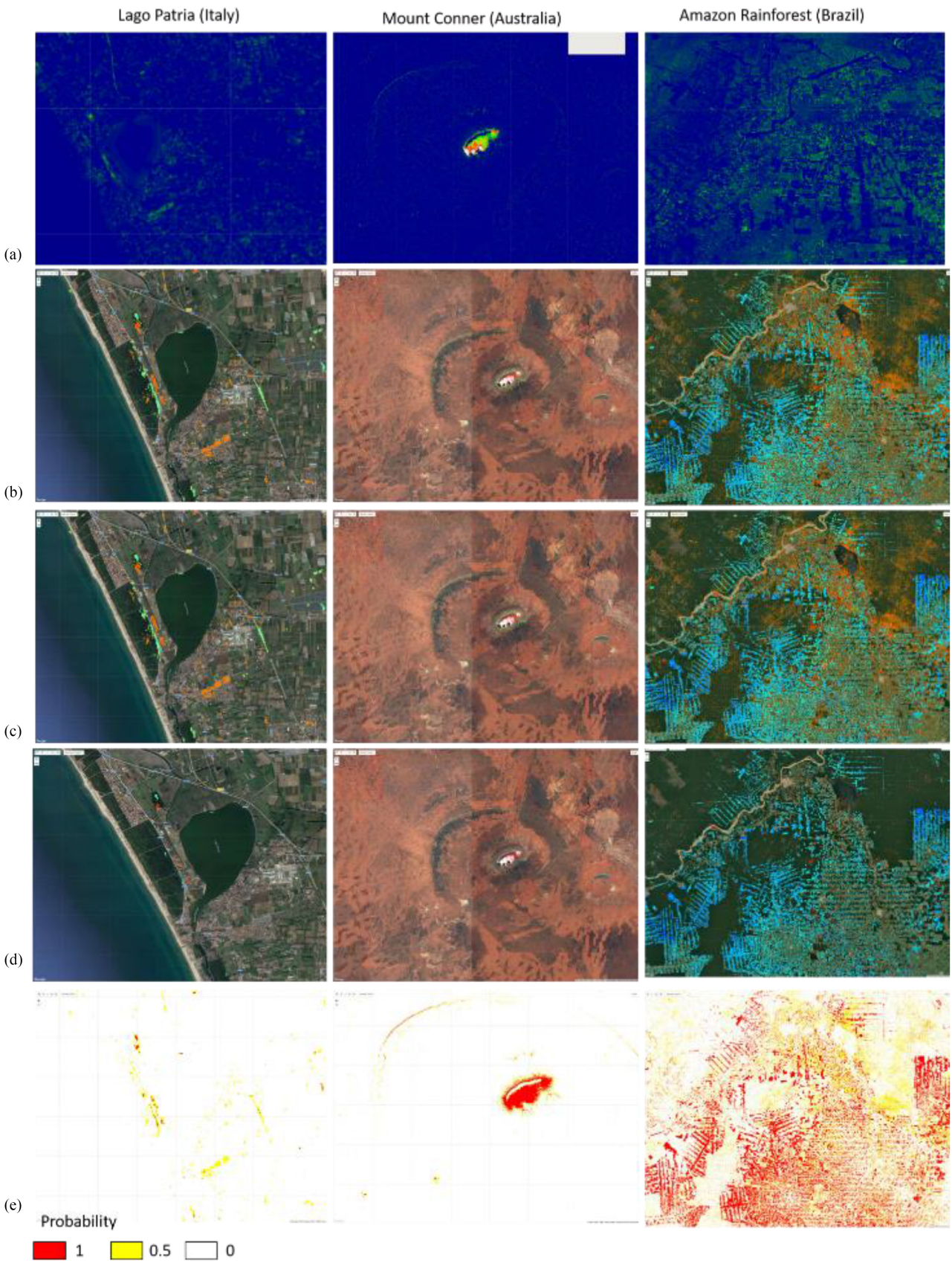

Fig. 8. Filtering strategies results: (a) nonfiltered DoD, (b) LoD, (c) UDE (confidence interval of 68%), (d) UDE (confidence interval of 95%), and (e) PM.

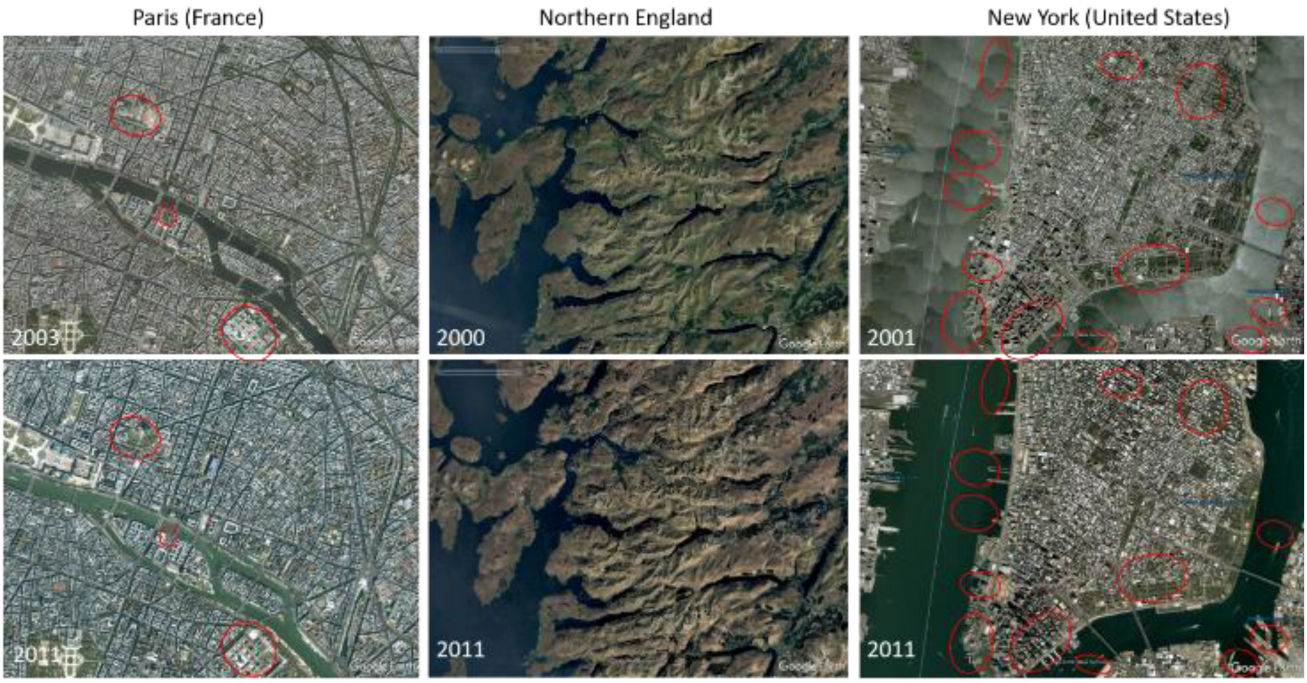

Fig. 9. Satellite images acquired from Google Earth Pro in two distinct periods and corresponding to two urban pilot sites [Paris, France (5411834.48 N, 452148.21 E) and New York, USA (4507413.11 N, 583784.41 E)] and a mountainous zone showing many outliers [Northern England, (6343367.38 N, 353822.85 E)]. Changes occurred in the considered period are highlighted with red circles.

Additionally, it offers other significant features, such as the availability of libraries of operators and machine learning scripts into the API; high flexibility that allows to custom in-house and specific algorithms; and an integrated catalog of open-source data. For these reasons, GEE is largely recognized as the most powerful tool in performing innovative analyses in the geospatial field. Therefore, it was adopted in the present study as the base computational framework to be coupled with open-source DEMs. As expected, it allowed processing open-source global DEMs in a short time and without any issues. As DEMs are already implemented in its catalog, the computational procedure was speeded up since they were directly imported in the API without downloading any product. Moreover, because of its flexibility, proper statistical approaches were implemented in computational codes to address specific needs raised during the analyses.

As a first point, the suitability of global DEMs in detecting changes was assessed. Four selected products were statistically analyzed and compared. The new version of AW3D30, released at the beginning of January 2021, appeared as the most accurate and realistic. Indeed, when compared to its previous version, the inherent inconsistency has been removed, as shown by their derivatives (see Fig. 5). Indeed, as previously underlined, errors due to lakes were totally cleaned out by masking water bodies during SRTM DEM V3, NASADEM, and AW3D30 (3.2) editing phase. Moreover, elevation overestimation has been also partially corrected (see Fig. 2). As promised by their producer, the latest AW3D30 version shows significant improvements both in terms of efficiency and effectiveness. It is worth noting that the present research represents the first study devoted to assessing AW3D30 (3.2) accuracy compared to its previous version as, also because of the released date, any pre-existing study was not developed yet.

Conversely, although NASADEM is considered the successor of SRTM, it does not provide substantial improvements overall the world. Indeed, in some cases, the improvements are minimal, as shown in Fig. 5. It appears less accurate than its predecessor for higher elevation analyses, as shown by the boxplots of Figs. 2 and 3, which confirm the outcomes already noted by previous research works but obtained with different approaches [21]. In [21], Uuemaa *et al.* evaluated the vertical accuracy of the largely widespread global DEMs, including SRTM DEM V3, NASADEM, and AW3D30 (3.2), by statistically comparing their values with a more accurate reference dataset on three regions: China, Estonian, and New Zealand. NASADEM showed a slightly higher average accuracy than its predecessor in all examined regions. Nevertheless, significant advances were not detected. An overall overestimation of the elevation was noted in all DEMs albeit it was more significant in NASADEM and AW3D30, as also highlighted in the present study (see Fig. 2).

Based on all these observations, the present research selected AW3D30 (3.2), and SRTM DEM V3 as the optimal DEM combination. They were integrated into the subsequent computational steps. To improve the quality and the reliability of the final products, outliers were identified and, then, cleaned out by using the Tukey method [51]. Detected outliers, even after DoD computation, were in the forested and mountainous zones (see Fig. 6) according to Uuemaa *et al.* [21]. That result is mainly due to the difficulty of SAR interferometry in producing an accurate DEM in the

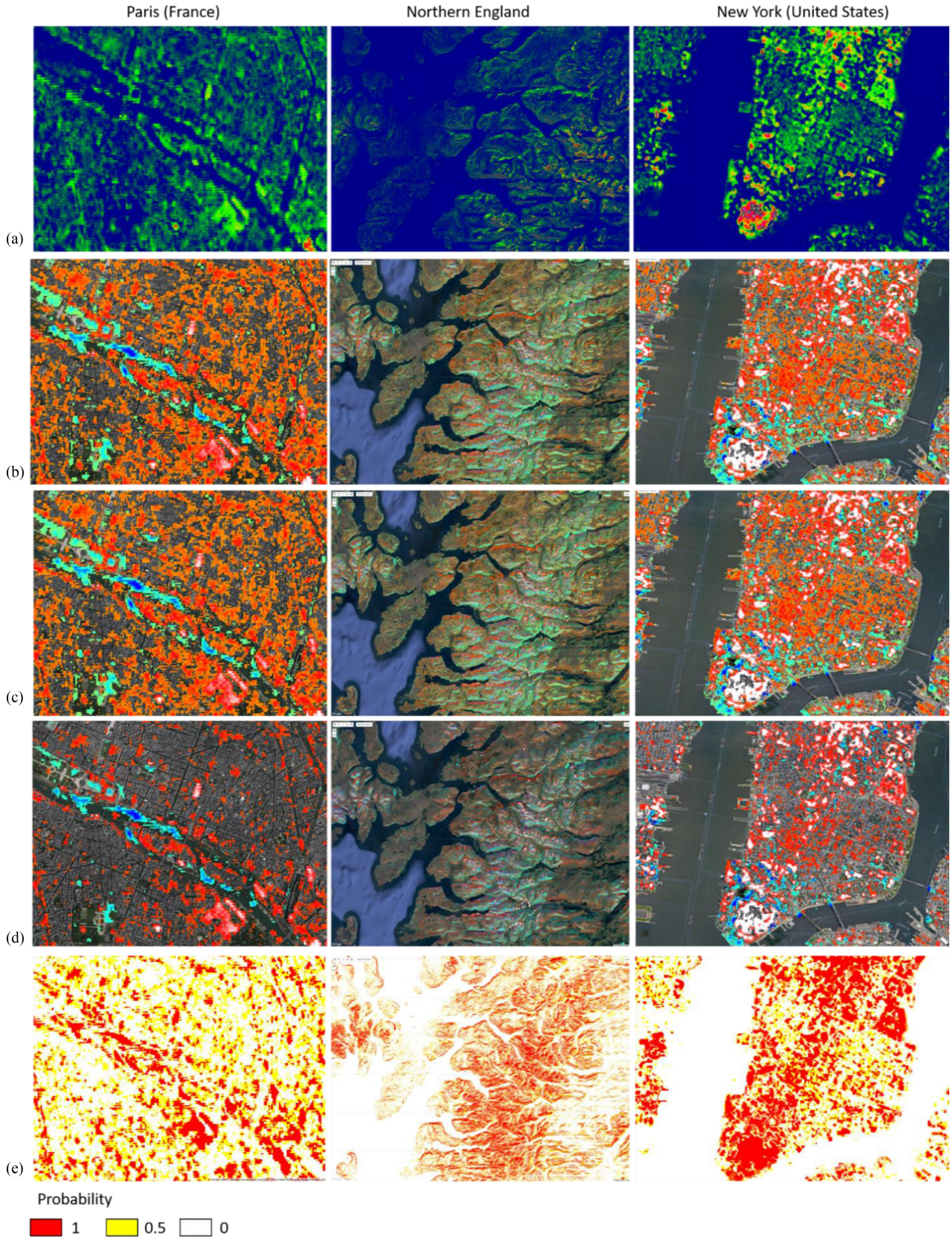

Fig. 10. Filtering strategies results: (a) nonfiltered DoD, (b) LoD, (c) UDE (confidence interval of 68%), (d) UDE (confidence interval of 95%), and (e) PM.

zones covered by trees because of a low detected point density. Vegetation features, like height and density, affect the percentage of the incoming radar scattered back to the sensor. In [21], Uuemaa *et al.* also analyzed the relationship between land cover types and global DEMs accuracy underlining their inappropriateness in forestry zones. For this reason, the DoD resulting from outliers removal showed an overall improvement even though not yet adequate to investigate 3-D changes over time. Thus, additional statistical strategies were introduced to filter the propagated error into the DoD. Lane *et al.* [26] enhanced the rapid diffusion of the combined noise from each singular DEMs into the final DoD. It is worth noting that this effect is even more relevant when one uses less accurate DEMs albeit this error is commonly neglected in change detection analysis. Therefore, due to poor global DEMs vertical accuracy, propagated error filtering resulted crucial in this study.

Among the three statistical proposed approaches (LoD, UDE, PM), PM appears as the optimal technique particularly because it allows integrating the information obtained using different confidence intervals. In fact, a confidence interval of 68% looks more appropriate to discriminate the changes in flatter areas (see Fig. 8, Lago Patria); while 95% is more suitable for mountainous, forestry (see Fig. 10, Mount Conner in Australia and Amazon Rainforest in Brazil) and urban areas (see Fig. 10, Paris and New York). None of the three methods reports satisfying outcomes in those areas characterized by many outliers as illustrated in Fig. 10. Moreover, as already noted by Brasington *et al.* [54] and James *et al.* [53], also in this case, the LoD method experienced the worst performance, mainly because it does not account for the probabilistic distribution of the error. According to those observations, the couple composed of SRTM DEM V3 and AW3D30 (3.2) shows the best results in detecting 3-D changes in rural, forestry, urban and mountainous areas. Conversely, the zones characterized by a large number of outliers (see Fig. 6) need a further filtering step (see Fig. 10). Such zones are mainly located along shorelines and mountainous areas. These results are in agreement with the ones obtained by: Misra *et al.* [57] who investigated the ability of SRTM DEM V3 and AW3D30 in extracting the building height in Yangon City; and by Nonomura *et al.* [58] who examined the suitability of AW3D30 product in assessing landslides in mountainous areas. In both cases, the authors stated that the input data were sufficient for their research goals.

V. Conclusion

This article has explored the possibility of detecting global changes combining recently released open-source global DEMs and GEE, an innovative, open, cloud computing platform devoted to treating geospatial big data. To the best of the author's knowledge, this is the first study that shows how appropriate filtering strategies allow reliable change detection analysis coupling together GEE with open-source global DEMs. In general, to perform global detection change analyses, the following three main issues can be encountered.

1) Lack of high-resolution DEMs covering the whole earth.
2) The standalone use of available medium-resolution global DEMs requires powerful operative systems.
3) When used, the global DEMs results are affected by accuracy heterogeneity, which reflects into unreliable outcomes.

This study faced all the above-mentioned problems showing how reliable and realistic results can be obtained on common operative systems using a wholly open-source environment thanks to the use of appropriate filtering strategies. The first issue was tackled using freely available, medium-resolution global DEMs, which provide good baseline information to describe the entire earth surface. The use of the GEE platform allowed to overcome the second constraint as it permits to fast and parallelly process large geospatial datasets. This feature speeded up the data treatment procedure permitting a fast outcomes production without any computational problems. Moreover, the GEE integrated catalog represented an additional saving-time advantage as it allowed to directly import the open-source DEMs in the API. Lastly, GEE flexibility allowed users to customize codes according to their specific needs. This feature allowed to overcome the third above-mentioned limitation. Indeed, in the present study, in-house Javascript codes were developed to assess the DEMs inherent inconsistencies and realism as well as to implement proper statistical and filtering strategies. Three filtering methods (i.e., LoD, UDE, and PM) were applied to filter potential outliers and error propagation.

As the main results of the proposed analyses, the use of AW3D30 (3.2), released at the beginning of January 2021, and SRTM DEM V3 represents the optimal combination to investigate 3-D changes over a period of 11 years. Nevertheless, in their corresponding DoD, a large number of Tukey's outliers, mainly located in the forestry and mountainous areas, were detected. This was essentially due to the different levels of accuracy of the input data in such zones. Indeed, all global DEMs overestimate the elevation over the whole earth even though this phenomenon is not homogeneously distributed. The correction of such artifact is extremely difficult as it implies the uncertainty increment and higher difficulty in assessing globally the elevation variability. After cleaning out the outliers, the application of further filtering strategies appeared essential to not misclassify the changes. Specifically, the PM approach resulted as the most performant. Confidence intervals of 68% and 95% are recommended to extract data from rural and mountainous/forestry/urban areas, respectively. The main outcome is that the combined use of medium-resolution global DEMs, GEE platform, and appropriate filtering strategies allows a realistic detection and 3-D modeling of changes at a global scale. Nevertheless, a particular need is outlined: much bigger effort should be paid in developing further correction filtering algorithms to locally fix global DoDs. Additionally, in order to investigate recent changes, more up-to-date products, not currently available, are required.

References

[1] P. W. Bogaart and P. A. Troch, "Curvature distribution within hillslopes and catchments and its effect on the hydrological response," *Hydrol. Earth Syst. Sci.*, vol. 10, pp. 925–936, 2006.

[2] A. Capolupo, L. Kooistra, and L. Boccia, "A novel approach for detecting agricultural terraced landscapes from historical and contemporaneous photogrammetric aerial photos," *Int. J. Appl. Earth Observ. Geoinf.*, vol. 73, pp. 800–810, 2018.

[3] K. J. McGuire *et al.*, "The role of topography on catchment-scale water residence time," *Water Resour. Res.*, vol. 41, no. 5, 2005, Art. no. W05002.

[4] I. D. Moore, R. B. Grayson, and A. R. Ladson, "Digital terrain modelling: A review of hydrological, geomorphological and biological applications," *Hydrol. Processes*, vol. 5, pp. 3–30, 1991.

[5] L. Polidori and M. El Hage, "Digital elevation model quality assessment methods: A critical review," *Remote Sens.*, vol. 12, no. 21, 2020, Art. no. 3522.

[6] I. S. Evans, "Geomorphometry and landform mapping: What is a landform?," *Geomorphology*, vol. 13, pp. 94–106, 2012.

[7] A. Capolupo, P. Nasta, M. Palladino, E. Cervelli, L. Boccia, and N. Romano, "Assessing the ability of hybrid poplar for in-situ phytoextraction of cadmium by using UAV-photogrammetry and 3D flow simulator," *Int. J. Remote Sens.*, vol. 39, no. 15/16, pp. 5175–5194, 2018.

[8] K. Holmes, O. Chadwick, and P. Kyriakidis, "Error in a USGS 30-meter digital elevation model and its impact on terrain modeling," *J. Hydrol.*, vol. 233, pp. 154–173, 2000.

[9] P. A. Shary, L. S. Sharaya, and A. V. Mitusov, "Fundamental quantitative methods of land surface analysis," *Geoderma*, vol. 107, pp. 1–32, 2002.

[10] G. B. Heuvelink, *Error Propagation in Environmental Modelling With GIS*. Boca Raton, FL, USA: CRC Press, 1998, pp. 1–150.

[11] J. Höhle and M. Potuckova, "Assessment of the quality of digital terrain models," *Eur. Spat. Data Res.*, vol. 60, no. 91, pp. 1–85, 2011.

[12] T. Podobnikar, "Methods for visual quality assessment of a digital terrain model," *SAPIENS*, vol. 2, pp. 1–10, 2009.

[13] M. Caprioli, M. Minchilli, A. Scognamiglio, and E. Tarantino, "3D modelling and metric analysis in architectural heritage: Photogrammetry and laser scanning," in *Proc. 6th Conf. Opt. 3-D Meas. Techn.*, Zurich, Switzerland, Sep. 22–25, 2003, p. 206.

[14] A. Vettore, S. Ponte, and N. Crocetto, "Space-based surface change detection with differential synthetic-aperture radar (SAR) interferometry: Potentialities and preliminary investigations," *Geomatica*, vol. 57, no. 3, pp. 326–334, 2003.

[15] E. Tarantino and B. Figorito, "Extracting buildings from true color stereo aerial images using a decision making strategy," *Remote Sens.*, vol. 3, no. 8, pp. 1553–1567, 2011.

[16] M. El Hage, E. Simonetto, G. Faour, and L. Polidori, "Effect of image-matching parameters and local morphology on the geomorphological quality of SPOT DEMs," *Photogramm. Rec.*, vol. 32, pp. 255–275, 2017.

[17] Y. Dong, H.-C. Chang, W. Chen, K. Zhang, and R. Feng, "Accuracy assessment of GDEM, SRTM, and DLR-SRTM in Northeastern China," *Geocarto Int.*, vol. 30, no. 7, pp. 779–792, 2015.

[18] Z. Walczak, M. Sojka, R. Wrózyński, and I. Laks, "Estimation of polder retention capacity based on ASTER, SRTM and LIDAR DEMs: The case of Majdany Polder (West Poland)," *Water*, vol. 8, no. 6, 2016, Art. no. 230.

[19] B. Purinton and B. Bookhagen, "Validation of digital elevation models (DEMs) and comparison of geomorphic metrics on the southern Central Andean Plateau," *Earth Surf. Dyn.*, vol. 5, no. 2, pp. 211–237, 2017.

[20] M. Varga and T. Bašić, "Accuracy validation and comparison of global digital elevation models over Croatia," *Int. J. Remote Sens.*, vol. 36, no. 1, pp. 170–189, 2015.

[21] E. Uuemaa, S. Ahi, B. Montibeller, M. Muru, and A. Kmoch, "Vertical accuracy of freely available global digital elevation models (ASTER, AW3D30, MERIT, TanDEM-X, SRTM, and NASADEM)," *Remote Sens.*, vol. 12, no. 21, 2020, Art. no. 3482.

[22] C. Hirt, "Artifact detection in global digital elevation models (DEMs): The maximum slope approach and its application for complete screening of the SRTM v4.1 and MERIT DEMs," *Remote Sens. Environ.*, vol. 207, pp. 27–41, 2018.

[23] J. Brasington and R. M. A. Smart, "Close range digital photogrammetric analysis of experimental drainage basin evolution," *Earth Surf. Processes Landforms, J. Brit. Geomorphol. Res. Group*, vol. 28, no. 3, pp. 231–247, 2003.

[24] A. Capolupo and L. Boccia, "Innovative method for linking anthropisation process to vulnerability," *World Rev. Sci. Technol. Sustain. Develop.*, vol. 17, no. 1, pp. 4–22, 2021.

[25] I. C. Fuller, A. R. G. Large, M. E. Charlton, G. L. Heritage, and D. J. Milan, "Reach-scale sediment transfers: An evaluation of two morphological budgeting approaches," *Earth Surf. Processes Landforms*, vol. 28, no. 8, pp. 889–903, 2003, doi: 10.1002/esp.1011.

[26] S. N. Lane, R. M. Westaway, and D. M. Hicks, "Estimation of erosion and deposition volumes in a large, gravel-bed, Braided River using synoptic remote sensing," *Earth Surf. Processes Landforms, J. Brit. Geomorphol. Res. Group*, vol. 28, no. 3, pp. 249–271, 2003.

[27] Google Earth Engine, 2015. Accessed: Apr. 19, 2020. [Online]. Available: https://earthengine.google.org

[28] D. J. Milan, G. L. Heritage, A. R. Large, and I. C. Fuller, "Filtering spatial error from DEMs: Implications for morphological change estimation," *Geomorphology*, vol. 125, no. 1, pp. 160–171, 2011.

[29] N. Gorelick, M. Hancher, M. Dixon, S. Ilyushchenko, D. Thau, and R. Moore, "Google Earth Engine: Planetary-scale geospatial analysis for everyone," *Remote Sens. Environ.*, vol. 202, pp. 18–27, 2017.

[30] L. Kumar and O. Mutanga, "Google Earth Engine applications since inception: Usage, trends, and potential," *Remote Sens.*, vol. 10, no. 10, 2018, Art. no. 1509.

[31] A. Capolupo, C. Monterisi, G. Caporusso, and E. Tarantino, "Extracting land cover data using GEE: A review of the classification indices," in *Proc. Int. Conf. Comput. Sci. Appl.*, Jul. 2020, pp. 782–796.

[32] Y. Feng, R. I. Negrón-Juárez, and J. Q. Chambers, "Remote sensing and statistical analysis of the effects of hurricane María on the forests of Puerto Rico," *Remote Sens. Environ.*, vol. 247, 2020, Art. no. 111940.

[33] A. Capolupo, C. Monterisi, and E. Tarantino, "Landsat images classification algorithm (LICA) to automatically extract land cover information in Google Earth Engine environment," *Remote Sens.*, vol. 12, no. 7, 2020, Art. no. 1201.

[34] A. Capolupo, C. Monterisi, C. Barletta, and E. Tarantino, "Google Earth Engine for land surface Albedo estimation: Comparison among different algorithms," *Proc. SPIE*, vol. 11856, pp. 51–63, 2021.

[35] M. A. Crowley, J. A. Cardille, J. C. White, and M. A. Wulder, "Multi-sensor, multi-scale, Bayesian data synthesis for mapping within-year wildfire progression," *Remote Sens. Lett.*, vol. 10, pp. 302–311, 2019.

[36] L. Wang *et al.*, "A summary of the special issue on remote sensing of land change science with Google Earth Engine," *Remote Sens. Environ.*, vol. 248, 2020, Art. no. 112002.

[37] P. Gong *et al.*, "Annual maps of global artificial impervious area (GAIA) between 1985 and 2018," *Remote Sens. Environ.*, vol. 236, 2020, Art. no. 111510.

[38] J. L. Safanelli *et al.*, "Terrain analysis in Google Earth Engine: A method adapted for high-performance global-scale analysis," *ISPRS Int. J. Geo-Inf.*, vol. 9, no. 6, 2020, Art. no. 400.

[39] A. Foni and D. Seal, "Shuttle Radar Topography Mission: An innovative approach to shuttle orbital control," *Acta Astron.*, vol. 54, pp. 565–570, 2004.

[40] T. G. Farr and M. Kobrick, "Shuttle Radar Topography Mission produces a wealth of data," *Eos Trans. Amer. Geophys. Union*, vol. 81, pp. 583–585, 2000.

[41] B. Rabus, M. Eineder, A. Roth, and R. Bamler, "The Shuttle Radar Topography Mission—A new class of digital elevation models acquired by spaceborne radar," *ISPRS J. Photogramm. Remote Sens.*, vol. 57, pp. 241–262, 2003.

[42] E. Rodríguez, C. S. Morris, and J. E. Belz, "A global assessment of the SRTM performance," *Photogramm. Eng. Remote Sens.*, vol. 72, no. 3, pp. 289–260, 2006.

[43] N. Kolecka and J. Kozak, "Assessment of the accuracy of SRTM C- and X-Band high mountain elevation data: A case study of the Polish Tatra Mountains," *Pure Appl. Geophys.*, vol. 171, pp. 897–912, 2014.

[44] A. Capolupo, C. Monterisi, M. Saponaro, and E. Tarantino, "Multi-temporal analysis of land cover changes using Landsat data through Google Earth Engine platform," in *Proc. 8th Int. Conf. Remote Sens. Geoinf. Environ.*, 2020, vol. 11524, Art. no. 1152419.

[45] NASA, "The Shuttle Radar Topography Mission (SRTM) collection user guide," 2015. Accessed: Nov. 20, 2020. [Online]. Available: https://lpdaac.usgs.gov/documents/179/SRTM_User_Guide_V3.pdf

[46] J. Takaku, T. Tadono, M. Doutsu, F. Ohgushi, and H. Kai, "Updates of 'AW3D30' AW3D30 Global Digital Surface Model with other open access datasets," *ISPRS Int. Arch. Photogramm. Remote Sens. Spatial Inf. Sci.*, vol. 43, pp. 183–89, 2020.

[47] T. Tadono, H. Ishida, F. Oda, S. Naito, K. Minakawa, and H. Iwamoto, "Precise global DEM generation by AW3D30 PRISM," *ISPRS Ann. Photogramm. Remote Sens. Spatial Inf. Sci.*, vol. 2, no. 4, pp. 71–76, 2014.

[48] NASA JPL, "NASA Shuttle Radar Topography Mission Global 1 Arc second DEM, version 3, NASA LP DAAC," 2013. [Online]. Available: http://doi.org/10.5067/MEaSUREs/SRTM/SRTMGL1.003

[49] Google Earth Engine, "Computation using images," 2021. Accessed: Feb. 3, 2021. [Online]. Available: https://developers.google.com/earth-engine/tutorials/tutorial_api_03

[50] J. M. Wheaton, J. Brasington, S. E. Darby, and D. A. Sear, "Accounting for uncertainty in DEMs from repeat topographic surveys: Improved sediment budgets," *Earth Surf. Processes Landforms, J. Brit. Geomorphol. Res. Group*, vol. 35, no. 2, pp. 136–156, 2020.
[51] J. W. Tukey, *Exploratory Data Analysis*. Reading, MA, USA: Addison-Wesley, 1977, pp. 131–160.
[52] J. R. Taylor, *An Introduction to Error Analysis: The Study of Uncertainties in Physical Measurements*, 2nd ed. Sausalito, CA, USA: Univ. Sci. Books, 1997.
[53] L. A. James, M. E. Hodgson, S. Ghoshal, and M. M. Latiolais, "Geomorphic change detection using historic maps and DEM differencing: The temporal dimension of geospatial analysis," *Geomorphology*, vol. 137, no. 1, pp. 181–198, 2012.
[54] J. Brasington, J. Langham, and B. Rumsby, "Methodological sensitivity of morphometric estimates of coarse fluvial sediment transport," *Geomorphology*, vol. 53, no. 3/4, pp. 299–316, 2003, doi: 10.1016/S0169-555X(02)00320-3.
[55] G. B. Norcliffe, *Inferential Statistics for Geographers*. London, U.K.: Hutchinson, 1977.
[56] H. M. Blalock, *Social Statistics*, 2nd ed. New York, NY, USA: McGraw-Hill, 1979.
[57] P. Misra, R. Avtar, and W. Takeuchi, "Comparison of digital building height models extracted from AW3D, TanDEM-X, ASTER, and SRTM digital surface models over Yangon City," *Remote Sens.*, vol. 10, no. 12, 2018, Art. no. 2008.
[58] A. Nonomura, S. Hasegawa, D. Kanbara, and T. Tadono, T. Chiba, "Topographic analysis of landslide distribution using AW3D30 data," *Geosciences*, vol. 10, no. 4, 2020, Art. no. 115.

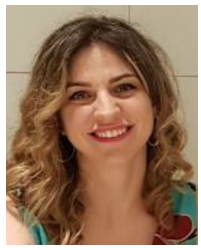

Alessandra Capolupo was born in Avellino, Italy, in 1987. She received the Ph.D. degree in sciences and technologies for the forest and environmental management from the University of Tuscia, Viterbo, Italy, in 2016.

From 2016 to 2019, she was a Postdoc Research Fellow and, after winning the STAR program in 2017, she moved to the University of Wageningen, Wageningen, The Netherlands. Since 2019, she has been an Assistant Professor of Geomatics (ICAR/06) with the Politecnico di Bari, Bari, Italy, where she is currently working on geomatics topics. Her research interests have been concerned with geomatics topics since 2013. She focused her attention on the most advanced technologies (such as GIS, photogrammetry, and remote sensing) and, she developed innovative algorithms and methods by exploiting the potentialities of big geospatial data.

Dr. Capolupo won some academic awards, such as the Best Paper Award, Young Scientist Award, Top Reviewers.